Radio-Frequency Size Effects in Single-Crystal Copper Plates

B. PERRIN, G. WEISBUCH,* AND A. LIBCHABER
Groupe de Physique des Solides de l'Ecole Normale Supérieure, Paris, France†
(Received 4 August 1969)

Radio-frequency size effects are studied in copper plates oriented perpendicular to the [100], [110], and [111] directions with the magnetic field **B** parallel and perpendicular to the sample surface. The contribution of different types of orbits to the transmitted signal is described. Point-by-point mapping of the Fermi surface is carried out and gives slight differences from previous work. When the magnetic field is normal to the plate, we observe all the theoretically predicted Gantmakher excitations. We give theoretical arguments to explain the occurrence of harmonics of Gantmakher oscillations, and the shift of the Gantmakher period across Doppler-shifted cyclotron-resonance edge in the [110] direction.

I. INTRODUCTION

SINCE the works of Gantmakher,[1,2] the radio-frequency size effect (RFSE) has become one of the most powerful methods of mapping the Fermi surface. The principle of the method is the following: At the surface of a pure single-crystal metal plate, a radio-frequency electromagnetic wave is excited within the skin depth, smaller at 4.2°K than the electron mean free path. In the presence of a magnetic field, the energy taken by the electron in the skin depth can be reradiated periodically along the electronic trajectory. The measurement of the magnetic field at which the electromagnetic wave is reemitted on the other side of the plate yields the dimensions of the Fermi surface. This paper is concerned with the study of RFSE in copper. Since we were especially interested in wave propagation, we have chosen to study the Gantmakher effects in a simple and well-known metal, copper, which has a Fermi surface sufficiently complex to allow the existence of a certain number of different nonlocal electronic excitations.

After a description of the experiment (Sec. II), we give in Sec. III the results of the experiments with the magnetic field parallel to the surface of the sample. These experiments allow us to relate the form of the electronic trajectories to the shape of the observed transmission spikes. They also give a precise measurement of the Fermi surface which can be compared with models given by Roaf[3] and Powell.[4] Section IV describes experiments with the magnetic field perpendicular to the sample surface. A theoretical calculation based on Powell's model of the Fermi surface of copper predicts quite well the periods of the observed Gantmakher oscillations. Short-period oscillations due to harmonics and the variation of the Gantmakher fundamental oscillations are explained at least qualitatively.

II. EXPERIMENTAL TECHNIQUE

A. Sample Preparation

For these experiments, one needs very high-purity copper single crystals with plane parallel surfaces. The purity has to be such that the electron mean free path l is greater than the sample thickness d ($l>d$).

We start with commercially available ASARCO copper ($\rho_{300°K}/\rho_{4.2°K}=300$). A Bridgmann technique is used to prepare a copper single crystal in a high-purity graphite crucible. The sample is then spark-cut x-ray oriented and mechanically planed. Following the method developed by Powell[4] and Gniewek[5] the sample is then annealed at 900°C under a reduced oxygen pressure (2×10^{-4} Torr) for about 48 h. The resistivity ratio $\rho_{300°K}/\rho_{4.2°K}$ stands typically between 5000 and 10 000. The oxide is removed by dissolution in hydrochloric acid and a slight mechanical lapping is applied to obtain a well-defined thickness, followed by electrolytic polishing to remove the damaged layers.

B. Experimental Setup

In order to observe sharp lines in $\mathbf{B}_{\parallel}$ geometry, the electromagnetic skin depth δ should be much smaller than the sample thickness d (the linewidth $\Delta B/B$ is proportional to δ/d).[2] This implies working at the highest possible frequencies compatible with the condition $\omega\ll\omega_c$ [6] ($\delta\propto\omega^{-1/3}$); we have been working in the frequency range 0.1–30 Mc/sec with the following:

The transmission technique developed by Grimes[7] using a single-side excitation up to 30 Mc/sec. In this setup, two coils, one for the excitation and the other for the detection, are placed on each side of the sample at a distance of about 0.1 mm: We use copper coils with 15 turns of 0.15-mm-diam wires. One of the main difficulties in using this technique is to reduce the leakage signal, which explains the complicated screening

* Present address: Faculté des Sciences de Luminy, 13—Marseille 9ème (France).

† Laboratoire associé au Centre National de la Recherche Scientifique. Mail address: 24, rue Lhomond, Paris 5ème (France).

[1] V. F. Gantmakher, Zh. Eksperim. i Teor. Fiz. **42**, 1416 (1962) [English transl.: Soviet Phys.—JETP **15**, 982 (1962)].

[2] V. F. Gantmakher and C. J. Görter, Progr. Low Temp. Phys. **5**, 181 (1967).

[3] D. J. Roaf, Phil. Trans. Roy. Soc. London **A255**, 135 (1962).

[4] R. L. Powell (private communications).

[5] J. J. Gniewek and A. F. Clark, J. Appl. Phys. **36**, 3358 (1965).

[6] So that there is no phase change of the electromagnetic field in the skin layer when the electron passes repeatedly across the skin layer. As a matter of fact, this condition does not seem to be so essential [see J. P. D'Haenens *et al.*, Phys. Letters **28A**, 312 (1968)].

[7] C. C. Grimes and S. J. Buschbaum, Phys. Rev. Letters **12**, 357 (1964).

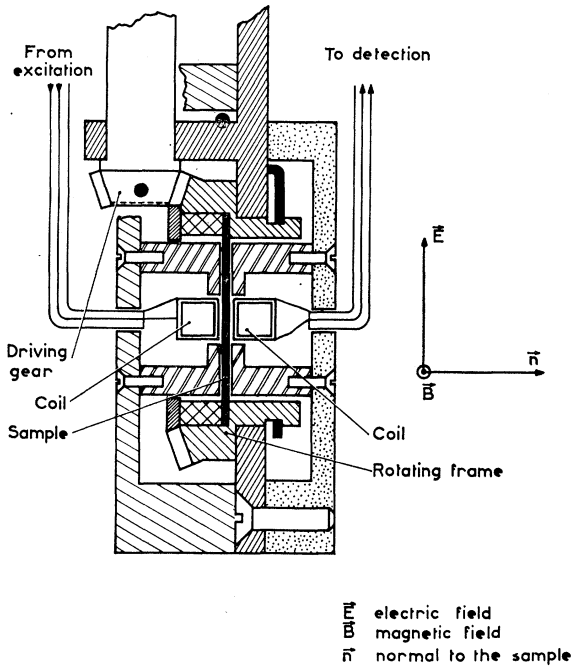

FIG. 1. Transmission setup.

system shown in Fig. 1. The main interest of the setup is that the sample can rotate in its plane (the vertical one), the two coils being fixed; this allows the study of propagation in a continuous range of crystal orientation, while keeping the excitation current at a constant angle with the magnetic field. The rotation of the magnet in the horizontal plane leads to all possible orientations of **B** towards the sample surface. We use a Rhode and Schwartz generator (SMLR 0.1–30 Mc/sec) and a HP 8405 A vector voltmeter, which gives the amplitude and phase of the transmitted signal (all the following recordings represent the variation of the phase difference between the incident and transmitted signals).

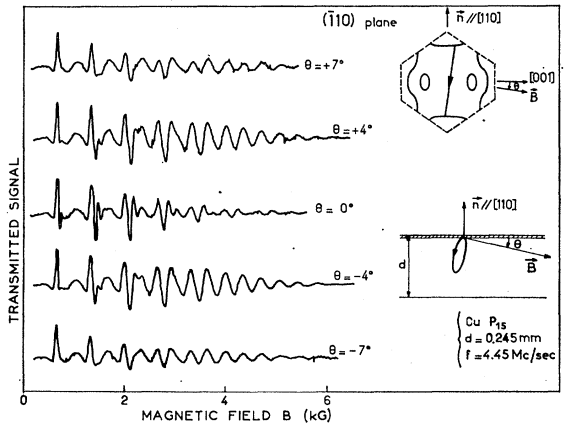

FIG. 2. Experiments with **B** parallel to the surface: closed trajectories. Tilting the field by a few degrees towards the sample surface increases the number of observable spikes.

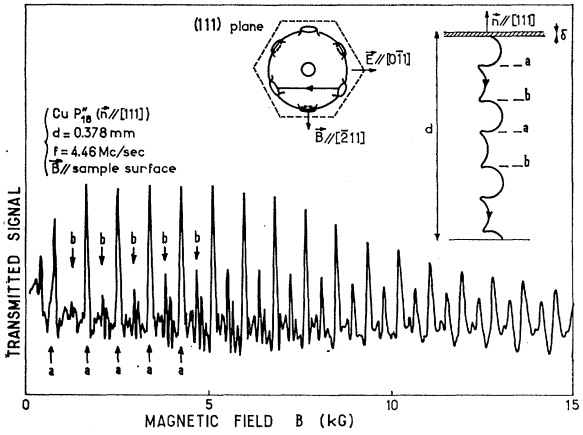

FIG. 3. Experiments with **B** parallel to the surface: open-orbit trajectories with effective points. The spikes are due to the effective points *a* and *b* of the open orbit.

The double-side excitation with a transistor marginal oscillator[8] in the frequency range 10–20 Mc/sec. The inductance of the tank circuit is a copper coil wound on the sample (20 turns of diam 0.2 mm). The derivative dR/dB of the real part of the surface impedance Z ($Z=R+iX$) is recorded as a function of the magnetic field B by a magnetic-field modulation technique and lock-in detection.[9]

All the experiments were carried out at 4.2°K, since decreasing the temperature below 4.2°K does not increase the mean free path l.

III. *B* PARALLEL TO SAMPLE SURFACE

In this geometry "effective electrons" play a dominant part. In one or several points of its orbit ("effective points"), an electron may have a velocity parallel to the surface. The energy coupling in the skin depth is at a maximum in that case; the energy is reradiated through the depth of the material into the thin layers where the electron velocity again becomes parallel to the surface.[2]

The distance at which the energy is reradiated is related to some dimension u of the trajectory. For different orbits corresponding to different sections of the Fermi surface, this dimension u is different: In the resulting interference the terms for which u is equal to its extremal value u_{ext} are going to be dominant. Electrons situated on such orbits are called "effective electrons." One observes splashes of transmission each time the thickness of the sample is a multiple of the dimension of the trajectory u_{ext}.

According to the magnetic field orientation with respect to the crystallographic axes, several types of splashes due to different types of trajectories can be observed in copper.

[8] B. Donnally and T. M. Sanders, Jr., Rev. Sci. Instr. **31**, 977 (1960).

[9] P. S. Peercy and W. M. Walsh, Jr., Phys. Rev. Letters **17**, 741 (1966).

A. Closed Trajectories

The occurrence of several field splashes into the sample is due to reexcitation: The current created at depth u by a first closed trajectory reexcites the surrounding electrons, so that electronic trajectories of velocity parallel to the surface at depth u give a current splash at depth $2u$, and so on. This reexcitation mechanism is not very effective and the splashes are soon attenuated after several reexcitations, when **B** is parallel to the surface, as shown by Peercy in potassium,[10] which has a spherical Fermi surface (FS).

Nevertheless, the mechanism can become important when a great percentage of the electrons limiting the skin depth participate in a resonant manner to the reexcitation. A nearly cylindrical FS fulfills this condition: For a (110) plate with the magnetic field parallel both to the surface and [001] direction, the major part of the electrons are describing "circles" of quasiconstant diameters corresponding to orbits situated between the necks (see Fig. 2, $\theta=0°$). Another way of getting slowly decreasing current sheets is obtained by a slight tilt of the magnetic field[11]; then the electrons, ineffective in creating the current sheets, do not play much part in determining the skin depth, since they soon drift out of it (see Fig. 2, $\theta=4°$).

B. "Effective" Periodic Open Trajectories

In this case, the signal can be transmitted without reexcitation, by electrons crossing over the sample. Effective points of the trajectory lead to current splashes. In this case damping is due to the limited electronic mean free path, and is related to the ratio l/d.[12] Such size effects can be due to electrons near the limiting point (in an inclined magnetic field), or to electrons on effective periodic open trajectories. Size effects with an effective periodic open trajectory exist in the (111) copper plane when $\mathbf{B}\|[\bar{2}11]$; for the plane intersecting the Fermi surface across two necks, a periodic open trajectory with mean direction perpendicular to the sample surface and period 2×1.809 $k_{\text{F.E.}}$ in k space appears ($k_{\text{F.E.}}\equiv$free-electron sphere radius$=1.363$ Å^{-1} at 4.2°K) (see Fig. 3).

C. "Ineffective" Periodic Open Trajectories

When there is no effective point on an orbit, the energy received in the skin depth is reradiated regularly all along the orbit; this case is similar to the observed effects when $\mathbf{B}\|\mathbf{n}$ (**n** normal to the sample surface), where one observes a sinusoidal transmitted signal.

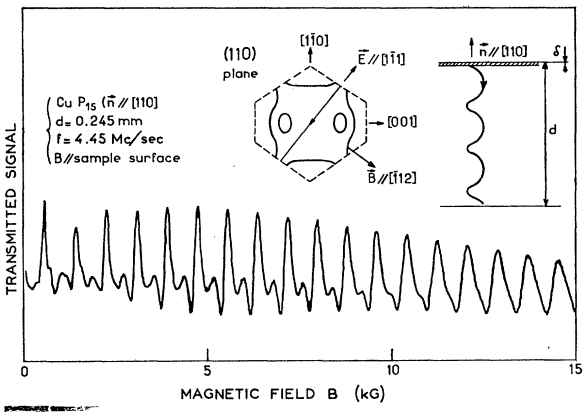

FIG. 4. Experiments with **B** parallel to the surface: open orbit with no effective point. The shape of the spikes becomes sinusoidal. (Compare with Fig. 3.)

For $\mathbf{B}\|$ to the sample, the sinusoidal variation is observed for "ineffective" periodic open trajectory with non zero mean normal velocity[13]: for instance, when $\mathbf{n}\|[110]$ and $\mathbf{B}\|[\bar{1}12]$, the orbit defined by the central cross-section goes through two necks symmetrical with respect to Γ and has no effective point. The recording (Fig. 4) shows an almost sinusoidal transmitted signal.

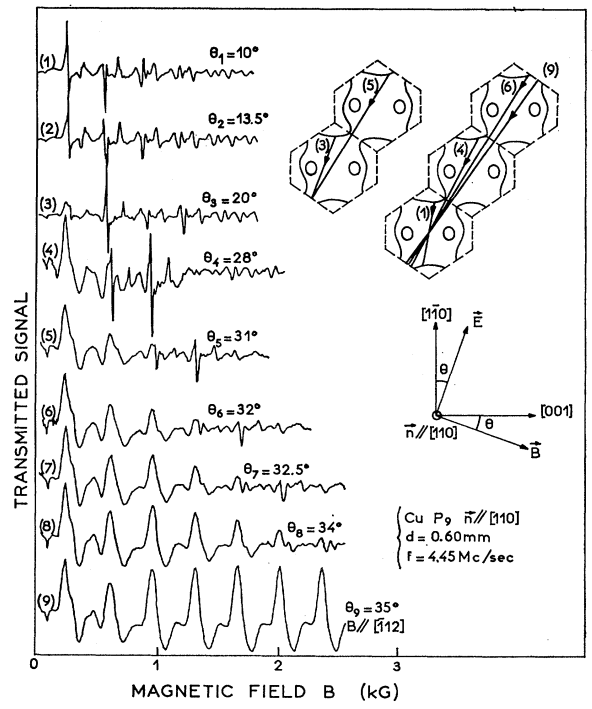

FIG. 5. Experiments with **B** parallel to the surface: transition between closed orbits and open orbits. When one varies the angle of the magnetic field towards the [001] axis, the spikes are due successively to one sphere orbits (θ_1,θ_2), two sphere orbits (θ_3), three sphere orbits (θ_4) ··· periodic open orbits (θ_9).

[10] P. S. Peercy, W. M. Walsh, Jr., L. W. Rupp, and P. H. Schmidt, Phys. Rev. **171**, 713 (1968).

[11] É. A. Kaner, Zh. Éksperim. i Teor. Fiz. **44**, 1036 (1963) [English transl.: Soviet Phys.—JETP **17**, 700 (1963)].

[12] V. F. Gantmakher and É. A. Kaner, Zh. Eksperim. i Teor. Fiz. **45**, 1430 (1963) [English transl.: Soviet Phys.—JETP **18**, 988 (1964)].

[13] A. A. Mar'yakhin and V. P. Naberezhnykh, Zh. Eksperim. i Teor. Fiz. Pis'ma v Redaktsiyu **3**, 205 (1966) [English transl.: Soviet Phys.—JETP Letters **3**, 130 (1966)].

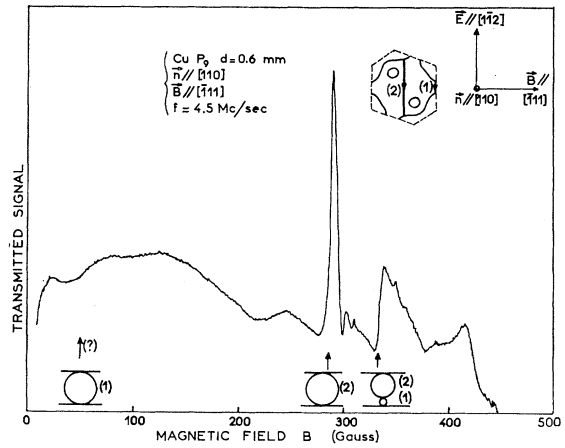

FIG. 6. Experiment with **B** parallel to the surface: reexcitation. The first splash is due to the neck orbit, the second to the belly orbit and the third to reexcitation of the neck trajectory by the current layer due to the belly trajectory (or inversely). The third splash is of greater amplitude than the first one because the electronic mean free path is much shorter on the neck orbit than on the belly orbit.

D. Transition between Closed and Periodic Open Trajectories

The experimental set-up allows us to study a transition between closed and open trajectories[14] by rotating the sample while **B** and **E** remain fixed (see Fig. 5). In the case of a (110) plate, we start with the magnetic field along the [001] axis, first obtaining a "belly" orbit [orbit (1) in Fig. 5] up to 23°, then a "two-belly" orbit [orbit (3) in Fig. 5], and continuously up to the periodic open orbit for $\theta = 35°$.

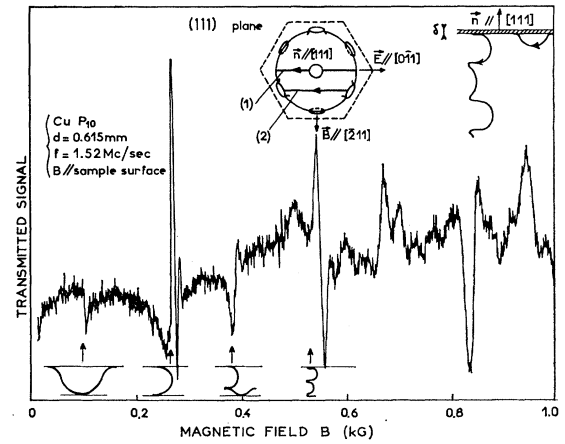

FIG. 7. Reexcitation between two periodic open orbits. The first splash is due to open orbit (1) moving parallel to the sample surface. The second, fourth, and sixth splashes are due to open orbit (2) moving perpendicular to the sample surface. The third, fifth, and seventh splashes are due to reexcitation of one orbit by the other.

[14] B. Perrin and A. Libchaber, in *Proceedings of the Eleventh International Conference on Low Temperature Physics* (University of St. Andrews Press, Scotland, 1968), p. 1191.

E. Reexcitation between Two Different Types of Trajectories

We show two examples of this effect,[15] one for closed orbits, one for periodic open orbits. For a magnetic field along the [1̄11] direction the layer formed by belly trajectories inside the metal reexcite neck trajectories[14] (Fig. 6). In the same geometry as in Fig. 3, but at lower magnetic field, Fig. 7 shows the different splashes due to the combination of two "effective" periodic open trajectories, one which sinks into the plate, and the other which moves parallel to the sample surface.

TABLE I. Extremal Fermi-surface dimensions for various orientations of magnetic field **B** in the (110) plane.

θ angle of **B** with [001] angle of k_0 with $k_{[\bar{1}10]}$	$k_0/k_{F.E.}$	Type of orbit (see Fig. 8)	Orbit center Origin of k_0
0°	0.920[a]	(1)	Γ
	0.690[b]	(6)	*L*
3°	0.922	(1)	Γ
	0.710	(6)	*L*
6°	0.927	(1)	Γ
9°	0.935	(1)	Γ
12°	0.946	(1)	Γ
15°	0.960	(1)	Γ
	1.880	(7)	*L*
18°	0.976	(1)	Γ
	1.905	(7)	*L*
21°	1.025	(1)	Γ
	1.960	(7)	*L*
24°	1.99	(7)	*L*
28.5°	3.15	(2)	Γ
31.5°	4.30	(8)	*L*
35°	1.108	p.o.o.[c]	
40.5°	3.14	(3)	Γ
43.5°	2.03	(10)	*L*
49°	1.015	(4)	Γ
52°	0.985	(4)	Γ
55°	0.970	(4)[d]	Γ
58°	0.960	(4)	Γ
61°	0.956	(4)	Γ
64°	0.954	(4)	Γ
67°	0.956	(4)	Γ
70°	0.965	(4)	Γ
	1.60	(11)	*L*
73°	1.50	(11)	*L*
76°	1.45	(11)	*L*
90°	0.753	(15)	off-centered[e]

[a] $k_{[\bar{1}10]}/k_{F.E.}$.

[b] Representative point *B* (see Fig. 8). $LB = 0.69$. $L'B = 0.215$, neck radius in the $[\bar{1}10]$ direction $= k_N{}_{[\bar{1}10]}/k_{F.E.}$.

[c] This orbit is used for the determination of the sample thickness (see Fig. 4).

[d] Apart from orbit (4) one observes excitation of neck orbit (12) by orbit (4). The following value of the neck radius in the [211] direction $k_N{}_{[211]}/k_{F.E.} = 0.15$.

[e] Centered at 0.75 $k_{F.E.}$ on $[\bar{1}10]$ axis.

[15] W. M. Walsh, Jr., C. C. Grimes, G. Adams, and L. W. Rupp, Jr., in *Proceedings of the Ninth International Conference on Low Temperature Physics* (University of Ohio Press, Columbus, 1964), p. 765.

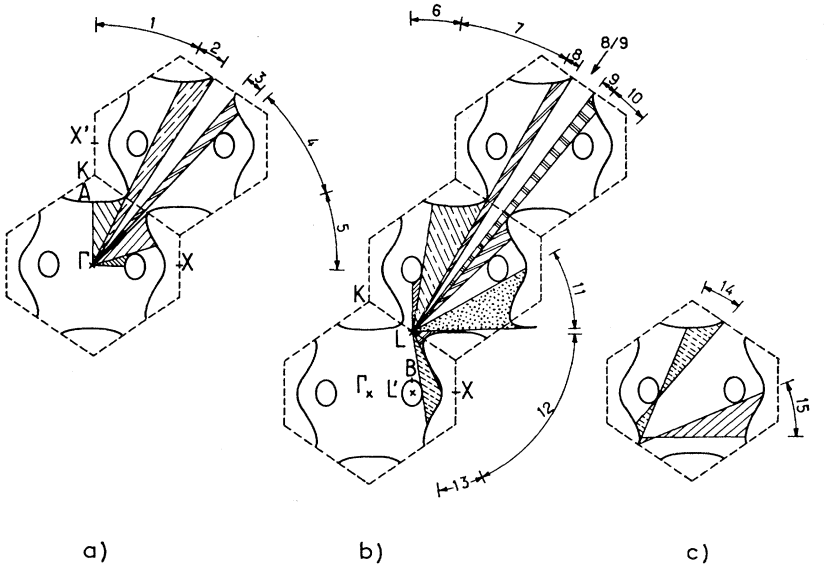

FIG. 8. Classification of electronic orbits when the magnetic field is in the [110] plane. [After J. F. Koch, R. A. Stradling, and A. F. Kip, Phys. Rev. **133**, A246 (1964).] (a) orbits centered on Γ; (b) orbits centered on L; (c) orbits with no center of symmetry.

F. Fermi-Surface Determination in (100), (110), (111) Planes

The main application of RFSE is the point-by-point mapping of the Fermi surface. Integrating the equation of motion

$$\hbar\dot{\mathbf{k}}=e\mathbf{V}\times\mathbf{B},$$

one gets

$$2k_0=(e/\hbar)dB_1.$$

$2k_0$ is the diameter of the orbit in k space in the direction $[\mathbf{n},\mathbf{B}]$ and B_1 is the magnetic field value corresponding to the first splash, where the diameter of the orbit equals the sample thickness.

Sample rotation allows us to study the orientation dependence of B_1 and therefore k_0, and thus to carry out a point-by-point mapping in the Fermi surface. The precision is limited by the uncertainties in d and B_1:

Mechanical measurement would lead to 1% precision in d; a better determination is achieved by using RFSE of orbits for which k_0 is related to the Brillouin-zone dimension, such as a periodic open orbit. Here the precision is about 0.2%, and is due to the fact that many periods can be pointed. The only limitation of the method is the existence of a periodic open orbit in the direction of interest.

The transmission spike has a linewidth $\Delta B/B\propto\delta/d$, which becomes sharper with increasing frequency. As suggested by Gantmakher,[2] we take for B_1 the starting point of the spike, which should be frequency independent. The precision of B_1 is 0.5%.

The resulting precision of k_0 is then 1%.

(110) Plane. Table I, Fig. 8. Spikes are due to the belly orbit (1) when $0<\theta<23°$, and (4) when $46°<\theta<63°$, where θ is the angle between **B** and [001] direction. For intermediate angles these orbits vary from multizone orbits to periodic open orbits (8/9, $\theta=35°$).

(100) Plane. Table II, Fig. 8. Three types of orbits: a belly orbit (1), a dog's bone orbit (6), and a noncentral orbit (15) are the dominant ones for size effects.

The results for (100) and (110) planes are plotted in Fig. 9.

(111) Plane. Table III, Fig. 10. Four different types of orbits are visible: (1′) dog's bone orbit; (2′) periodic open orbit with mean velocity parallel to the sample surface; (3′) and (4′) two-zone orbits. Only orbits (3′) and (4′) are used in Fermi-surface determination,

TABLE II. Extremal Fermi-surface dimensions for various orientations of the magnetic field **B** (in the (001) plane).

θ angle of **B** with [110] angle of k_0 with [$\bar{1}$10]	$k_0/k_{\text{F.E.}}$	Type of orbit (see Fig. 8)	Orbit center Origin of k_0
0°	0.886[a]	(5)	X
	0.859	(15)	off-centered
2°	0.887	(5)	X
5°	0.888	(5)	X
	0.863	(15)	
8°	0.867	(15)	
11°	0.895	(5)	X
	0.880	(15)	
17°	0.956	(1)	Γ
20°	0.960	(1)	Γ
23°	0.964	(1)	Γ
26°	0.970	(1)	Γ
29°	0.983	(1)	Γ
32°	0.994	(1)	Γ
35°	1.011	(1)	Γ
38°	1.033	(1)	Γ
41°	1.045	(1)	Γ
44°	1.050	(1)	Γ
45°	1.051[b]	(1)	Γ

[a] Representative point A of k_0. $X'A=0.886$, $\Gamma A=k_{[110]}/k_{\text{F.E.}}=0.923$ (to be compared with direct determination in Table I, $\theta=0$).
[b] $k_{[010]}/k_{\text{F.E.}}$.

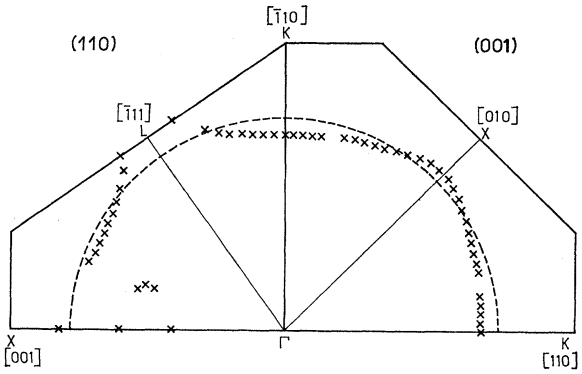

FIG. 9. Plot of experimental data in the [110] and [001] planes. The dashed line is the free-electron Fermi sphere. Crosses are from Tables I and II.

since for (1′) and (2′) the two effective points are nonsymmetric.

The data of extremal Fermi surface dimensions k_0 in Tables I, II, and III are mean values deduced from size-effect studies with several samples of different thickness (0.3 mm$<d<$0.8 mm), and by using for the (100) and (110) planes the two experimental techniques (marginal oscillator and transmission experiment). In the (111) plane (Table III) only the transmission technique has been used for two different samples. There is general agreement between our results and the latest work on the copper Fermi surface. An analytical expression of the Fermi surface of copper has been given by Roaf[3] using mainly Pippard's anomalous-skin-effect data[16] and Schoenberg's de Haas–van Alphen data.[17] A more precise numerical representation has been given by Powell[4] and is based on Roaf's equation, Bohm-Easterling's magnetoacoustic measurements[18] and Koch *et al.* cyclotron resonance data.[19] However, we disagree with these experimental results on two points:

(1) A rather strong anisotropy of the neck radius is observed. We find $0.16k_{\text{F.E.}}$ when it is measured along a line passing through the center of the hexagonal Brillouin zone face and the midpoint of one edge ($k_{N[211]}$) and $0.21k_{\text{F.E.}}$ along a line passing through the center and one corner ($k_{N[110]}$). These two values are not deduced from direct measurements: one is measured from the reexcitation of the neck orbit [orbit (12) in Fig. 8] by the belly orbit (4) (see Table I, $\theta=55°$); the other is deduced from the size effect due to the four-cornered rosette (6).

(2) The measured value of $k_{[110]}$ is $0.92k_{\text{F.E.}}$ which is smaller than all other measurements. For instance, Bohm-Easterling magnetoacoustic measurements[18] yield $k_{[110]}=0.956k_{\text{F.E.}}$ We emphasize this result which we obtain from five samples of different thickness. All the results lie in the interval $(0.916–0.926)k_{\text{F.E.}}$.

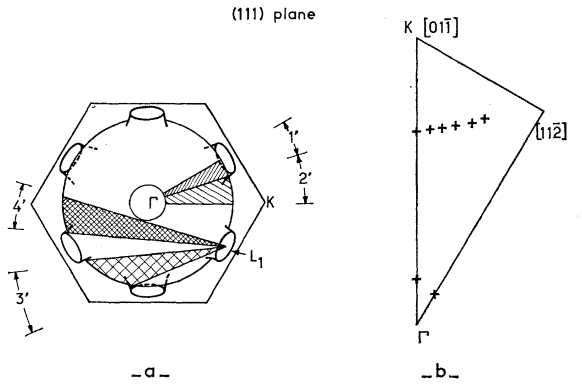

FIG. 10. (a) Classification of electronic orbits in the [111] plane. (b) Plot of experimental data taken from Table III.

IV. *B* NORMAL TO SAMPLE SURFACE

A. Theory

Starting from the following expression of the electric field E inside a metal:

$$E_{\pm}(z)=-\frac{1}{\pi}\,\frac{-E'_{\pm}(0)}{}\int_0^{+\infty}\frac{dq(e^{iqz}+e^{-iqz})}{q^2-i\mu_0\sigma_{\pm}(q)\omega},$$

where the z axis is normal to the surface, $\pm$ subscripts refer to the two circular polarizations, $E'=\partial E/\partial z$, $\sigma_{\pm}(q)$ is the wave-vector-dependent conductivity, and μ_0 the vacuum-magnetic permeability, Gantmakher

TABLE III. Extremal Fermi-surface dimensions for various orientations of the magnetic field **B** (in the (111) plane).

θ angle of **B** with [2$\bar{1}\bar{1}$] angle of k_0 with $k_{[01\bar{1}]}$	$k_0/k_{\text{F.E.}}$	Type of orbit [see Fig. 10(a)]	Orbit center Origin of k_0
0°	0.708[a]	(2′)	
	1.809	p.o.o.[b]	
6°	1.90	(4′)	L_1
8°	1.88	(4′)	L_1
	1.49	(3′)	L_1
10°	1.88	(4′)	L_1
	1.45	(3′)	L_1
12°	1.84	(4′)	L_1
	1.40	(3′)	L_1
14°	1.88	(4′)	L_1
	1.33	(3′)	L_1
16°	1.90	(4′)	L_1
	1.29	(3′)	L_1
30°	0.883[c]	(1′)	X

[a] This allows a second determination of $k_{N[110]}=k_{[110]}-0.708\ k_{\text{F.E.}}=0.21\ k_{\text{F.E.}}$.
[b] This orbit is used for the determination of the sample thickness (see Fig. 3).
[c] This value of k_0 is used for a new determination of $k_{N[211]}=0.16\ k_{\text{F.E.}}$.

[16] A. B. Pippard, Phil. Trans. Roy. Soc. London **A250**, 325 (1957).
[17] D. Shoenberg, Phil. Trans. Roy. Soc. London **A255**, 85 (1962).
[18] H. V. Bohm and V. J. Easterling, Phys. Rev. **128**, 1021 (1962).
[19] J. F. Koch, R. A. Stradling, and A. F. Kip, Phys. Rev. **133**, A240 (1964).

and Kaner[20] (GK) have shown that in a metallic slab perpendicular to the magnetic field two different types of electromagnetic excitations can propagate:

(1) Solutions of the dispersion equation $q^2-i\mu_0\sigma(q)\omega=0$, which we call dispersive waves.

(2) Branch points of $\sigma(q)$. These branch points are due to the helical electron trajectories inside the sample. Each trajectory corresponds to a section of the Fermi surface by a plane perpendicular to the magnetic field (k_z constant) and has a definite spatial periodicity $u(k_z)$. $u(k_z)$ is defined by

$$u(k_z)=(h/eB)(\partial S/\partial k_z).$$

When $u(k_z)$ has an extremum value u_0 as a function of k_z this gives a branch point of $\sigma(q)$ for

$$q=2\pi/u_0.$$

The branch point corresponds to an excitation propagating inside the metal; these excitations are called "Gantmakher excitations."

We use a model of Gantmakher excitations given in a recent paper[21] for spherical Fermi surfaces, to explain our effects. In this calculation one first considers the electric field due to the dispersive waves. This electric field may be written

$$E(z)=E_0e^{iqz},$$

where q is the solution of the dispersion relation. We write that an electron takes momentum from this field as long as it remains in the skin depth:

$$dp_{z'}=eE_0e^{iqz'}(dz'/v_z).$$

$dp_{z'}$ is the increase of momentum received at depth z'. But, because of the rotation of the momentum of the electron along its helical path, the extra momentum also rotates at the same frequency as the electron. Thus $dp_{z'}$ becomes at the depth z,

$$dp_{zz'}=(eE_0/v_z)e^{iqz'}e^{(2i\pi/u)(z-z')}dz'.$$

All the momentum received at different depths z' from 0 to z contributes to the current at z. The current density is then

$$j(z)=\int_0^z\frac{eE_0}{mv_z}e^{iqz'}e^{(2i\pi/u)(z-z')}dz'.$$

For $z>\delta$ where δ is the attenuation length of the dispersive mode:

$$j(z)=\frac{eE_0}{mv_z}\frac{1}{i(q-2\pi/u)}e^{(2i\pi/u)z}. \quad (1)$$

This is the contribution of one electronic orbit; one then has to take into account the contribution of all orbits of different u. The final result gives a sinusoidal current whose period is the extremal value of u. Since E_0 is an oscillating function of time with frequency ω, so is $j(z)$, and thus an oscillating electric field is excited, which is precisely the Gantmakher excitation. From Eq. (1) we see that the Gantmakher excitation has a maximum amplitude when $q-2\pi/u$ is minimum. This means that Gantmakher excitations are launched by the dispersive waves. This launching is a resonant process giving a maximum amplitude when the wave vectors of the two waves are equal.

In conclusion, a transmission experiment in a copper plate with the magnetic field perpendicular to the plate gives oscillations of the detected signal with magnetic field (see Fig. 16). Starting from high magnetic fields one observes several regions:

(1) Above the Doppler-shifted cyclotron resonance[22] (DSCR) edge one observes dispersive waves such as helicon waves which amplitude increases with magnetic field.

(2) A series of Gantmakher excitations existing in different field regions in the vicinity of their maximum amplitude where the relation $q=2\pi/u$ is verified.

The first explanation of the existence of several Gantmakher excitations with different periods is to suppose that there exist several values of k_z of extremal $u(k_z)$. This model[14] does not agree with the theoretical calculation of $\partial S/\partial k_z$ based on a numerical model of the copper Fermi surface given by Powell,[4] which clearly limits the number of different possible extrema (see Fig. 11 and Table IV).

In accordance with other results,[23] we have to come back to the idea of excitation of harmonics of Gantmakher excitations, in a manner similar to the occurrence of harmonics in diamagnetic cyclotron resonance.[24]

We consider a nonspherical Fermi surface such as copper, which has nonetheless three types of symmetry axes: [100] fourfold axis, [110] binary axis, and [111] threefold axis. When the magnetic field is directed along one of these axes, the orbits in k space have the symmetry of the axis whose order is α.

The problem is the following: When the electron goes down the plate it follows a periodic path of period u, but because all the parameters v_z, $v_\perp$ at each point φ [25] of the orbits are not constant, the angle of rotation

[20] V. F. Gantmakher and É. A. Kaner, Zh. Eksperim. i Teor. Fiz. **48**, 1572 (1965) [English transl.: Soviet Phys.—JETP **21**, 1053 (1965)]. See also G. A. Baraff, Phys. Rev. **167**, 625 (1968).

[21] G. Weisbuch and A. Libchaber, Phys. Rev. Letters **19**, 498 (1967).

[22] Helicon waves are absorbed by DSCR when there exist electrons such that $2\pi/u=q$. q is the wave vector of the propagating helicon mode. The highest value of the magnetic field allowing this is the DSCR edge [see E. A. Stern, Phys. Rev. Letters **10**, 91 (1963)].

[23] J. F. Koch (private communication); I. P. Krilov, Zh. Eksperim. i Tero. Fiz. **54**, 1738 (1968) [English transl.: Soviet Phys.—JETP **27**, 934 (1968)].

[24] H. J. Zeiger, B. Lax, and R. N. Dexter, Phys. Rev. **105**, 495 (1957).

[25] φ is defined by $d\varphi=\omega_c dl$, where the origin of time is arbitrary. We see that during a cyclotron period $\Delta\varphi=2\pi$.

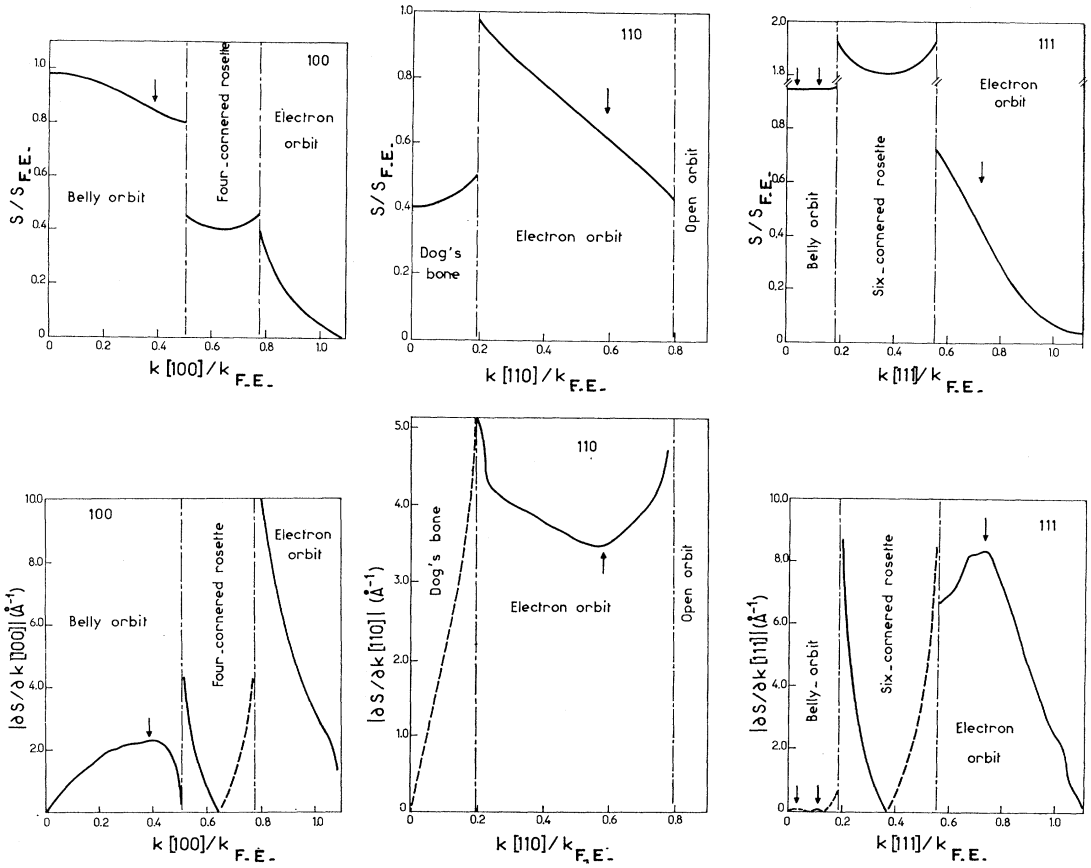

FIG. 11. Theoretical values of S and $\partial S/\partial k_z$. These values given for the three main directions of the magnetic field are calculated from Powell's numerical model of copper Fermi surface. Extrema of $\partial S/\partial k_z$ indicated by the arrows on the curves correspond to the observed fundamental periods of Gantmakher excitations.

of the extra momentum is not proportional to z but can fluctuate periodically about $(2\pi/u)z$.

In the first approximation, the momentum taken by an electron is proportional to the skin depth of the dispersive wave over the velocity of the electron along the z axis,

$$dp \approx (\delta/v_z)eE_0,$$

which means that the electron would see a constant

TABLE IV. Theoretical and experimental values of $\partial S/\partial k_z$.

Axis∥to **B**, **n**, and z axis	Theoretical values deduced from Powell's Fermi surface $\left(\frac{\partial S}{\partial k_z}\right)_{\text{th}}$ (Å^{-1})	$k_z/k_{\text{F.E.}}$	Experimental value $\left(\frac{\partial S}{\partial k_z}\right)_{\text{exp}}$ (Å^{-1})	Comments
[100] ($\alpha=4$)	2.27	0.38	2.3	Fundamental excitation $m=0$
			0.76	Harmonic 3
[111] ($\alpha=3$)	8.39	0.725	7.6	Fundamental excitation $m=0$
			1.8	Harmonic 4
	0.071	0.035	0.35	
	0.0214	0.115	0.23	
[110] ($\alpha=2$)	3.46	0.585	3.70	Fundamental excitation $m=0$
			1.90	?
			0.735	Harmonic 5

field while it is in the skin depth; the momentum gained is the integral of the force during the time it is in the skin depth.

When we consider a given orbit in phase space, v_z depends upon the position of the electron on the orbit. We refer to this position by the coordinate φ. Thus electrons situated at different φ have different v_z, and thus take different dp. Moreover, the corresponding dp does not rotate in the same manner: This rotation depends on the rotation of the velocity perpendicular to the magnetic field when φ varies. Thus we suppose that the current due to all the electrons of an orbit with a given k_z is given by the following integral:

$$j_x(z)=\oint \frac{\delta}{v_z(\varphi_0)} eE_0 f_x(z,\varphi_0)d\varphi_0,$$

where φ_0 is the position of one electron in its orbit when $z=0$, and $f_x(z,\varphi_0)$ describes the variation of the projection on the x axis of the rotating extra momentum when z increases. $f_x(z,\varphi_0)$ is periodic in z (period u) and in φ_0 (period 2π). The integral is over a period of φ_0.

Since $1/v_z(\varphi_0)$ and $f_x(z,\varphi_0)$ are periodic in φ_0 and z, we decompose these functions in Fourier series in φ_0 and z and keep only those terms for which the integral does not vanish. In fact, not all terms of the Fourier series are nonzero, because of the symmetry of the orbit of order α.

$$\frac{1}{v_z(\varphi_0)}=\sum_n A_n e^{in\alpha\varphi_0}, \quad n=0,\pm1,\ldots.$$

The decomposition is a little more complicated for $f_x(z,\varphi_0)$ because, as the electron moves along the orbit, the extra momentum rotates in the same manner as $\mathbf{v}_\perp$, the velocity in the plane of the orbit. This is due to the relation

$$\hbar\dot{\mathbf{k}}=e\mathbf{v}\times\mathbf{B}.$$

Then

$$f_x(z,\varphi_0)=\sum_m B_m(\varphi_0)e^{i(m\alpha\pm1)2\pi z/u}.$$

The $\pm$ appears because, while a vector parallel to the axis of rotation is conserved by a rotation of π, a vector perpendicular to this axis is reversed.

The symmetries $B_m(\varphi_0)$ are less evident, so we write it

$$B_m(\varphi_0)=\sum_p C_{mp}e^{ip\varphi_0}.$$

We finally get

$$j_x(z)=\sum_{n,p,m} e^{i(m\alpha\pm1)2\pi z/u}\oint A_n C_{mp} e^{i(n\alpha+p)\varphi_0}d\varphi_0,$$

which is nonzero when $n\alpha+p=0$. Thus the current density corresponding to one section of a given k_z is composed of Fourier components of period $u(m\alpha\pm1)^{-1}$. When one adds the contribution of all the sections of the Fermi surface there also the fundamental and its

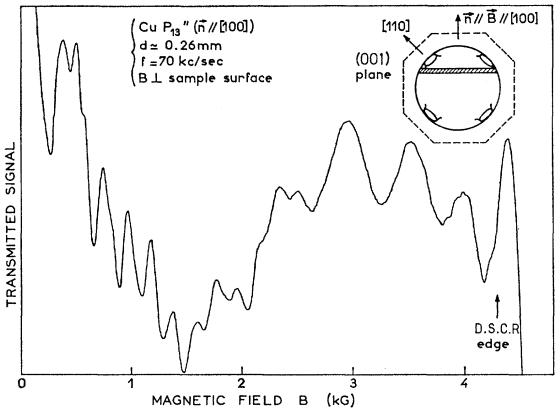

FIG. 12. Experiment with **B** along the [100] axis and perpendicular to the sample surface. Below DSCR edge, two periods are visible, the fundamental and the third harmonic. The shaded belt represents in this figure, and in Figs. 13–16 the electrons carrying the Gantmakher excitation.

harmonic are extremal for the same k_z. Thus the period of the observed harmonics do not differ from an entire fraction of the fundamental.

Of course the electromagnetic wave excites precisely the harmonic whose wave vector is closest to its own wave vector.

B. Experimental Results

Harmonics

The results are presented in Table IV.

(1) [100] (Fig. 12). Starting from high magnetic fields one first observes helicon waves of very large amplitude; below the DSCR edge, large GK oscillations of period proportional to $\partial S/\partial k_z=2.3$ Å^{-1} start and at lower magnetic fields, the third harmonic ($4m-1$, where $m=1$) appears and becomes dominant for $B<2$ kG. The deduced value of $\partial S/\partial k_z$ is in good agreement with the theoretical one calculated from

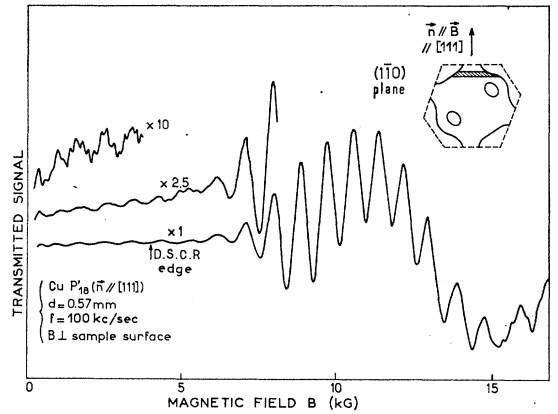

FIG. 13. Experiment with **B** along the [111] axis and perpendicular to the sample surface. Superimposed on helicon signal one sees the oscillations of the fundamental and at lower field, the fourth harmonic.

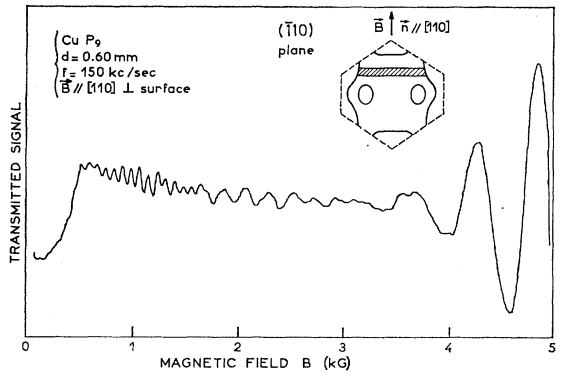

FIG. 14. Experiment with **B** along the [110] axis and perpendicular to the sample surface. Three periods are visible: at high field, the fundamental; at lower field, the fifth harmonic; in the intermediate region, possibly, the third harmonic.

Powell's F.S. (2.27 Å^{-1}); it also agrees with Boyd and Gavenda's[26] ultrasonic measurements (2.28 Å^{-1}).

(2) [111] (Fig. 13). In this direction, where there is a strong compensation, the helicon wave vector is small (the number of carriers giving a Hall voltage is 8% of the total number of carriers) and the helicon wave is responsible for the slow background oscillations. The GK oscillations coexist then with the helicons and give a period corresponding to $\partial S/\partial k_z = 7.6$ Å^{-1}. The theoretical value, $\partial S/\partial k_z = 8.39$ Å^{-1}, is found extremal for the electron belt near the inflexion region of the upper neck. At lower magnetic fields, the fourth harmonic ($3m+1$, where $m=1$) appears. At still lower fields, two other periods start, and we associate them with the other theoretically predicted extremal values of $\partial S/\partial k_z$ (see Table IV). In this region of k_z the imprecisions of the Fermi surface lead to important errors in calculating $\partial S/\partial k_z$ which could account for the discrepancy between the theoretical and experimental values.

(3) [110] (Fig. 14). This figure only shows GK oscillations (helicon waves appear for $B>8$ kG). Starting from larger fields, we first have large oscillations due to the extremum of $\partial S/\partial k_z$ (the discussion of the value of the period is reported in the next chapter). Harmonic 5 appears at low magnetic fields ($2m+1$, where $m=2$). The other oscillations at intermediate field could be the third harmonic (see the remark at the end of the theoretical section).

Current Splashes with B Normal to Sample Surface

The fact that v_z is not constant during the helical motion of the electron leads not only to the appearance of harmonics, but also to narrow field spikes when $v_z \approx 0$. Of course they appear when the orbit size is much larger than the skin depth i.e., at small magnetic fields. We observe them for **B**||[100] and [110]. Figure 15 presents this effect for **B**||[110]: Let us note that splashes occur not only at magnetic field values equal to nB_0 (where B_0 is the magnetic field period of GK oscillations at higher magnetic fields), but also at nB_0/α (where α is the order of symmetry of the axis).

Interaction between GK Oscillations and Helicon Waves

We return now to the main GK oscillations in the [110] direction: a very striking phenomenon appears. The GK oscillations are present on both sides of the DSCR edge, and the period varies between two extreme periods (as reported in[14])

$B_m = 400$ G (period at higher magnetic field),

$B_M = 580$ G (period at lower magnetic field)

for the sample used in Figs. 14–16. As it was correctly stated by Antoniewicz *et al.*,[27] the "pure" GK oscillations correspond to B_m in the region where the helicon is present with a wavelength very different from the orbit periodicity. B_m corresponds to the theoretical value $\partial S/\partial k_z = 3.46$ Å^{-1} (see Table IV and Ref. 27). A further confirmation is the occurrence of low magnetic fields splashes caused by the same electrons at values of $B = \frac{1}{2}nB_m$ (Fig. 15).

We recall that in the [100] and [111] directions, no change in period is observed. One sees from Fig. 11 that $\partial S/\partial k_z$ has a minimum value only in the [110] direction. This suggests the following explanation: when the helicon waves and GK signal coexist ($B > B_{\text{DSCR edge}}$), they do not interact because of the large wavelength mismatch and the GK oscillations are launched in the skin depth by the other circularly polarized mode. After the edge ($B < B_{\text{edge}}$), the resonant damping of the helicon increases the skin depth and thus tends to

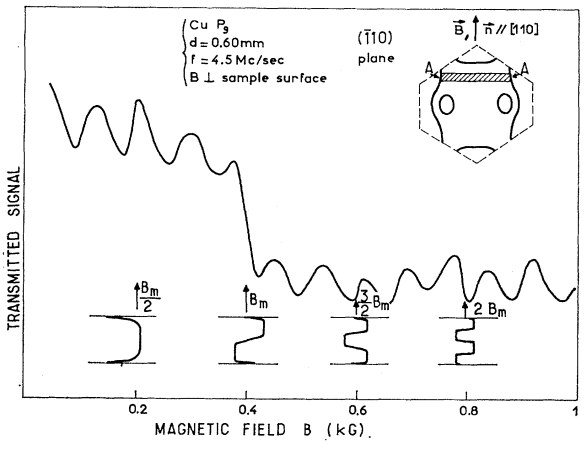

FIG. 15. High-frequency experiment with **B** along the [110] axis and perpendicular to the sample surface. Using high frequency allows us to observe transmission spikes due to effective points A of the orbit. These spikes occur at magnetic field $\frac{1}{2}nB_m$, where B_m is the period of the fundamental Gantmakher excitation. The sinusoidal background is the Gantmakher fifth harmonic.

[26] J. R. Boyd and J. D. Gavenda, Phys. Rev. **152**, 645 (1966).

[27] P. A. Antoniewicz, L. T. Wood, and J. D. Gavenda, Phys. Rev. Letters **21**, 998 (1968).

launch excitations of larger $\partial S/\partial k_z$, which is possible only if $\partial S/\partial k_{z\,\mathrm{ext}}$ is minimum ([110] direction). Thus our explanation of the change in period is related to a shift towards larger $\partial S/\partial k_z$ of the electrons creating the GK oscillations. Our tentative explanation is reinforced by the following argument: The Gantmakher period in the [110] direction is continuously varying from B_m to $B_M=1.4B_m$, and for this orbit, the k_z-dependent quantity $\partial S/\partial k_{[110]}$ goes from $(\partial S/\partial k_z)_{\min}$ $=3.46$ Å^{-1} to $1.5(\partial S/\partial k_z)_{\min}=5.2$ Å^{-1}.

When $\partial S/\partial k_{z\,\mathrm{ext}}$ is a maximum ([100],[111]), the GK oscillations are always caused by the less misadapted electrons, i.e., the electrons with $(\partial S/\partial k_z)_{\max}$.

Dispersive Waves and Open Orbits in [110] Direction

The large amplitude oscillations that appear above the DSCR edge are helicon waves whose wave vector is a solution of the dispersion equation. With the magnetic field pointing along the [110] direction, because of the presence of open orbits, the conductivity tensor can be written in the local regime in a simplified way[28]:

$$\sigma=\sigma_0\begin{bmatrix}\beta^2 & \beta & 0\\ -\beta & \beta^2+\alpha & 0\\ 0 & 0 & 1\end{bmatrix}.$$

σ_0 is the conductivity in the absence of magnetic field, $\beta=1/\omega_c\tau$, and α, which is independent of magnetic field, represents the "proportion" of open orbits and is defined by the equation

$$\alpha=\frac{1}{2\pi v}\int_{-k_0}^{k_0}(\Delta k_x)^2dk_z.$$

Δk_x is the momentum gained by an electron during an open-orbit period, and v is the volume of the Fermi surface.

For **B** along the [110] axis

$$\alpha\sim 0.04,$$
$$\beta\sim 0.04/B,\quad B \text{ in Tesla}.$$

The theory of wave propagation for such a conductivity tensor is now well known.[29–31] Two regions have to be distinguished (Fig. 16):

$\alpha<\beta$ (*low fields*). Between the DSCR edge and the point $\alpha=\beta$ the effect of open orbit is not dominant, and one observes propagation of helicon waves. The transmitted signal is not very different in the presence of open orbits ($\theta=0°$), and in their absence ($\theta=2°$). One can see in the region where $\alpha>\beta^2$ the influence of open orbits on the attenuation of the wave.

$\alpha>\beta$ (*high fields*). Open orbits are predominant and the electromagnetic wave can exist as two linearly polarized modes that are rapidly attenuated inside the metal.

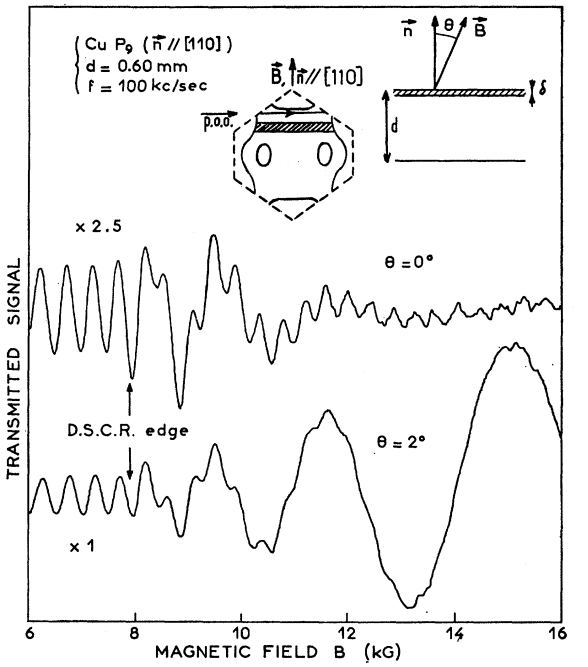

FIG. 16. Wave propagation above DSCR edge. When $\theta=2°$ the magnetic field is tilted from [110] and there exist no open orbits: helicon wave of increasing amplitude with increasing field can propagate. When $\theta=0$, helicon waves are rapidly attenuated by electrons moving along open orbits.

V. CONCLUSION

We have been able to observe a number of different types of Gantmakher excitations and to relate them to the corresponding electronic orbits. A precise determination of the section of the Fermi surface by the three main planes (100), (110), and (111) was carried out: one of the interesting results is the evidence for the anisotropy of the neck radius previewed by theoretical calculations.[32] We have used our knowledge of the shape of the Fermi surface of copper to verify our theoretical arguments explaining some features of Gantmakher excitations, due to the nonsphericity of the Fermi surface:

(1) The occurrence of harmonics of Gantmakher oscillations.

(2) The period shift of the Gantmakher oscillation

[28] The nonsphericity of the Fermi surface creates other smaller terms that will not change the results quantitatively.

[29] S. J. Buschbaum and P. A. Wolff, Phys. Rev. Letters 15, 406 (1965).

[30] C. C. Grimes, G. Adams, and P. H. Schmidt, Phys. Rev. Letters 15, 409 (1965).

[31] G. Weisbuch, Thèse d'Etat, Paris, 1967 (unpublished).

[32] G. A. Burdick, Phys. Rev. Letters 7, 156 (1961).

below the DSCR edge when it corresponds to a minimum of $\partial S/\partial k_z$.

These two effects are closely related to the resonant launching of the Gantmakher excitations by the dispersive waves.

ACKNOWLEDGMENTS

It is a great pleasure to thank Dr. R. L. Powell for sending us his computed copper Fermi surface, and C. Laroche for technical assistance in sample preparation and experiments.

PHYSICAL REVIEW B VOLUME 1, NUMBER 4 15 FEBRUARY 1970

Third-Order Elastic Constants of Zinc*

K. D. SWARTZ† AND C. ELBAUM
Department of Physics, Brown University, Providence, Rhode Island 02912
(Received 4 August,1969)

The complete set of ten third-order elastic constants of zinc was determined from measurements of the hydrostatic and uniaxial stress dependence of ultrasonic velocity. The experiments were carried out using the two-specimen interferometric method on appropriately oriented single crystals of zinc. The magnitudes of C_{222} and C_{111} are largest, followed by C_{333} which is less than one-third of C_{222}, whereas C_{144} is the smallest of all. All the constants except C_{155} are negative. The "macroscopic" values of the Grüneisen γ for zinc are evaluated.

INTRODUCTION

CRYSTAL anharmonicity determines or affects various properties of solids, for example, thermal expansion, thermal conductivity, temperature dependence of elastic constants, and attenuation of high-frequency waves. The theoretical treatment of crystal anharmonicity usually involves an expansion of the strain energy of a crystal in terms of finite strains. The coefficients of terms of a given order in this expansion are conveniently defined as the corresponding-order elastic constants. Alternatively second-, third-, and higher-order elastic constants can be defined as the second, third, and higher derivatives of the free energy (isothermal constants) or of the internal energy (adiabatic constants) of the crystal with respect to finite strains. From the knowledge of higher-order elastic constants it is possible, in some cases, to estimate the relative importance of various contributions to the interatomic potential as well as to determine the general form of this potential.

The present work is concerned with the determination of the third-order elastic constants (TOEC) of zinc. As far as the authors are aware, this is the first report of a complete set of TOEC for a metal with the hexagonal-close-packed crystal structure.

The TOEC were obtained from measurements of the hydrostatic and uniaxial stress dependence of sound velocity in single crystals. In the case of solids containing mobile dislocations, such measurements must be carried out in a manner such as to eliminate or subtract the added effects of dislocations. The dependence of the attenuation of the propagating wave on amplitude and on static stress is a sensitive indicator of dislocation effects.[1] This method was used, therefore, to ascertain whether dislocations were affecting the measurements. In the present study all propagation modes having a shear component of stress in the (0001) plane were found to be sensitive to dislocations when zinc crystals of nominal purity 99.999% were used. No such sensitivity was found, however, in zinc crystals containing 0.5% (atomic) aluminum. For all the other propagation modes used, dislocation effects were not detected in either the high-purity zinc or the zinc containing the aluminum. As is shown later, the TOEC obtained on the two types of crystals were the same, within the experimental uncertainty of the measurements.

EXPERIMENTAL PROCEDURE AND RESULTS

The zinc single crystals were grown from the melt with predetermined orientation. Two sets of single crystals were prepared, one of 99.999% pure zinc, the other using the same starting material with the addition of 0.5% (atomic) aluminum to the melt. Precautions were taken to insure uniformity of composition for the second set of samples. All the specimens were in the shape of parallelepipeds; those of higher purity had the approximate dimensions $1.5\times1.5\times2.0$ cm, the ones of lower purity had the approximate dimensions $0.9\times1.1\times1.4$ cm. They were prepared from the respective single crystals by cutting and planing on a spark

* Work supported in part by the National Science Foundation.
† Summer visitor under National Science Foundation grant. Permanent address: Department of Physics W.P.I., Worcester, Mass. 01609.

[1] R. Truell, C. Elbaum, and B. B. Chick, *Ultrasonic Methods in Solid State Physics* (Academic Press Inc., New York, 1969).